P H Y S I C A L   R E V I E W   L E T T E R S

Electron Transport through Single Mn$_{12}$ Molecular Magnets

H. B. Heersche,[*] Z. de Groot, J. A. Folk,[†] and H. S. J. van der Zant

Kavli Institute of Nanoscience, Delft University of Technology, Lorentzweg 1, 2628 CJ Delft, The Netherlands

C. Romeike and M. R. Wegewijs

Institut für Theoretische Physik A, RWTH Aachen, 52056 Aachen, Germany

L. Zobbi,[1] D. Barreca,[2] E. Tondello,[2] and A. Cornia[1]

[1]*Department of Chemistry, University of Modena and Reggio Emilia and INSTM, via G. Campi 183, I-41100 Modena, Italy*
[2]*ISTM-CNR, Department of Chemistry, University of Padova and INSTM, Via Marzolo 1, I-35131 Padova, Italy*

We report transport measurements through a single-molecule magnet, the Mn$_{12}$ derivative [Mn$_{12}$O$_{12}$(O$_2$C-C$_6$H$_4$-SAc)$_{16}$(H$_2$O)$_4$], in a single-molecule transistor geometry. Thiol groups connect the molecule to gold electrodes that are fabricated by electromigration. Striking observations are regions of complete current suppression and excitations of negative differential conductance on the energy scale of the anisotropy barrier of the molecule. Transport calculations, taking into account the high-spin ground state and magnetic excitations of the molecule, reveal a blocking mechanism of the current involving nondegenerate spin multiplets.

During the past few years, it has been demonstrated that metallic contacts can be attached to individual molecules, allowing electron-transport measurements to probe their intrinsic properties. Coulomb blockade and the Kondo effect, typical signatures of a quantum dot, have been observed at low temperature in a single-molecule transistor geometry [1–3]. In the Coulomb blockade regime, vibrational modes of the molecule appear as distinct features in the current-voltage (I-V) characteristics [4–6]. Conformational, optical, or magnetic properties of molecules may also affect electron transport. With respect to the latter, an interesting class of molecules is formed by the single-molecule magnets (SMMs). These molecules show magnetic hysteresis due to their large spin and high anisotropy barrier, which hampers magnetization reversal. The prototypal SMM, Mn$_{12}$ acetate, has total spin $S = 10$ and an anisotropy barrier of about 6 meV [7,8]. Spin excitations play an important role in the magnetization reversal process through quantum tunneling of the magnetization (QTM) [9]. Although the electronic and magnetic properties of SMMs have been studied intensively on bulk samples and thin films [10–14], the effect of the high-spin ground state on electron transport in isolated molecules remains an unexplored topic [15].

In this Letter, we discuss transport through individual SMMs that are weakly coupled to gold electrodes (see Fig. 1). Experimental data show low-energy excited states with a strong negative differential conductance (NDC) and regions of complete current suppression (CCS). We have modeled tunneling through a single Mn$_{12}$ molecule, taking into account its magnetic properties. Sequential tunnel processes can result in spin blockade of the current, providing a possible explanation for the observed NDC and

CCS. This effect is different from conventional spin blockade [16,17], where there is no spin anisotropy.

We use the single-molecule magnets [Mn$_{12}$O$_{12}$(O$_2$C-R-SAc)$_{16}$(H$_2$O)$_4$] (Mn$_{12}$ in the rest of the text), where $R = \{C_6H_4, C_{15}H_{30}\}$. Both are tailor-made Mn$_{12}$-acetate derivatives [8]. These molecules feature thiol groups in the outer ligand shell and, consequently, exhibit a strong affinity for gold surfaces [13,18]. Besides ensuring robust tethering of the clusters to the surface, the ligands are also believed to serve as tunnel barriers, so that the molecule is only weakly coupled electronically to the gold. We assume that its magnetic properties are conserved in the vicinity of gold electrodes. The diameter of the molecule (core plus ligands) is about 3 nm for $R = C_6H_4$ and 5 nm for $R = C_{15}H_{30}$. In this
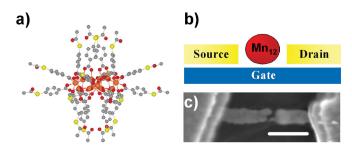

FIG. 1 (color). (a) Side view of a Mn$_{12}$ molecule with tailor-made ligands containing acetyl-protected thiol end groups ($R = C_6H_4$). Atoms are color labeled: manganese (orange), oxygen (dark red), carbon (gray), sulfur (yellow). The molecule diameter is about 3 nm. (b) Schematic drawing of the Mn$_{12}$ molecule (red circle) trapped between electrodes. A gate changes the electrostatic potential on the molecule enabling energy spectroscopy. (c) Scanning electron microscopy image of the electrodes. The gap is not resolvable. Scale bar corresponds to 200 nm.

Letter, we focus on the transport features that are measured on the $R = C_6H_4$ derivative, which is depicted in Fig. 1(a).

Electromigration [19] produced the nanometer-scale gaps in which the molecules were trapped. We fabricated thin (~10 nm) gold wires (width 100 nm, length 500 nm) on top of a Al/Al_2O_3 gate using e-beam lithography. The wires were contacted by thick (100 nm) gold leads. Samples were cleaned in acetone and isopropanol, descummed with an oxygen plasma, then soaked in a 0.1 mM Mn_{12} solution containing a catalytic amount of aqueous ammonia (to promote deprotection of the SAc groups; see Ref. [18]) for at least 1 h. After taking a sample out of the solution, it was dried in a nitrogen flux and mounted in a 4He system with a 1 K pot. The bridges were electromigrated in vacuum at room temperature by ramping a voltage across them while monitoring the current using a series resistor of 10 Ω. The junctions broke at about 1 V.

After breaking, the samples were cooled down to 4 K, and the junction conductances were measured as a function of gate voltage. Although about 10% of 200 junctions showed Coulomb blockade related features, only four samples were stable enough for detailed measurements [20]. In Fig. 2(a), we plot the differential conductance G as a function of gate (V_g) and bias voltage (V_b) for one such device ($T = 3$ K, $R = C_6H_4$). The lines separating the conducting regions from the diamond-shaped Coulomb blockade regions have different slopes for the three different charge transport regions. Within orthodox Coulomb blockade theory, this implies that the transport regions belong to different quantum dots, since the capacitance to the environment is assumed constant for each dot. However, for molecular quantum dots, it is not possible to rule out that these three regions come from three different charge states of the same molecule. Kubatkin *et al.* found that the charge distribution—and, therefore, also the capacitance—of a (large) molecule depends on its charge state [3]. In either scenario, however, the current in the nonoverlapping transport regions is determined by a single molecule.

Lines in transport regions running parallel to the diamond edges correspond to the onset of transport through excited states of the molecule. We have observed an excitation at 14 ± 1 meV in all 6 of the stable transport regions that were observed in the four samples. This excitation is indicated with arrows in Figs. 2(c)–2(f) and 3(a) and appears to be a fingerprint of the molecule. Its origin can be vibrational since the Raman spectrum exhibits strong peaks beyond this energy, which are associated with vibrations of the magnetic core of the molecule [21]. A fingerprint is needed, since metal grains that are formed during electromigration can mimic the transport properties of single molecules [22–24]. Moreover, we have studied the electromigration process extensively and found that the gap size can be tuned by the total series resistance [25]. A relatively large series resistance (200 Ω) has been used to create a gap larger than ~1 nm. Using this technique,
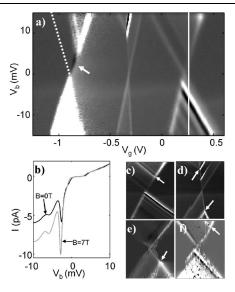

FIG. 2. (a) Differential conductance (gray scale) as a function of gate voltage (V_g) and bias voltage (V_b) ($T = 3$ K, $R = C_6H_4$). A region of complete current suppression (left degeneracy point, arrow) and low-energy excitations with negative differential conductance (right degeneracy point) are observed. The dashed line near the left degeneracy point indicates the suppressed diamond edge (gray scale from -0.8 [black] to 1.4 nS [white]). (b) $I - V_b$ at the gate voltage indicated in (a) with a line. NDC is clearly visible as a decrease in $|I|$ upon increasing $|V_b|$. Upon applying a magnetic field, current is increased for negative bias. (c)–(f) Same as (a) for 4 transport regions in which the 14 meV excitation is indicated with arrows. Bias voltage ranges are $V_b = \pm 30$ mV, $V_b = \pm 20$ mV, $V_b = \pm 25$ mV, and $V_b = \pm 15$ mV, respectively. (c) and (d) are the right and center charge transport regions of the sample in (a), respectively. (e) and (f) are measured in devices with the $R = C_{15}H_{30}$ ligands.

we did not measure any conductance up to 1 V in 50 control samples without molecules deposited.

The focus of this Letter is on transport features at low energy ($\lesssim 5$ meV): a region of CCS and a strong NDC excitation line in the stability diagrams. Both are visible in Fig. 2(a). At the left degeneracy point in this figure, the current is fully suppressed at positive bias voltage above the left diamond edge (dashed line). Transport is restored beyond an excitation that lies at 5 meV. Remarkably, the right diamond edge *does* continue all the way down to zero bias, defining a narrow strip (~1 mV wide) where transport is possible. In the right conductive regime in Fig. 2(a), two excitations at an energy of 2 and 3 meV are the most pronounced features. The 2 meV excitation is visible as a bright line with positive differential conductance (PDC), the 3 meV excitation as a black line (NDC). The strength of the NDC is clearly visible in the $I - V_b$ plot in Fig. 2(b).

PDC and NDC excitations at 2 and 3 meV were also observed in a different device; see Fig. 3. Although the details varied from sample to sample, these features were consistently observed. In all cases, the 14 meV excitation is visible, suggesting that this feature originates in the core of the molecule. We emphasize that we have never observed
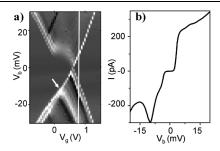
FIG. 3. (a) Differential conductance (gray scale) as a function of gate voltage (V_g) and bias voltage (V_b) for another device ($T = 1.5$ K, $R = C_6H_4$) in which the 2 and 3 meV excitations are also observed (negative bias). The 14 meV excitation is indicated by a white arrow. The origin of the step in the diamond edge at positive bias is unclear but most likely not related to the magnetic properties of the molecule (gray scale from -3 [black] to 10 nS [white]). (b) $I - V_b$ along the line in (a).

FIG. 4 (color online). Model calculations. (a) Energy diagram of the S_z states for the electronic ground state ($\alpha = 0$, blue) and first excited state ($\alpha = 1$, red) of the neutral molecule ($N = n$). (b),(c) Differential conductance (gray scale from -0.8 [black] to 1 a.u. [white]) modeling CCS (b) and NDC (c). Parameters are listed in Ref. [30].

similar low-energy features (CCS or NDC) in bare gold samples or in samples with other molecules deposited, despite measuring over 1000 junctions in total.

The observations of CCS and NDC lines at low energy do not follow in a straightforward way from conventional Coulomb blockade theory. For a qualitative comparison to the experimental data, we have developed a standard sequential tunneling model that incorporates the spin-Hamiltonian description of the high-spin ground state of Mn_{12} and its ladder of spin excited states (see Fig. 4). Both the total spin of the molecule S and its projection M on the intrinsic anisotropy axis of the molecule (the z axis) are taken into account. Briefly, the spin-selection rules $|\Delta S|, |\Delta M| = \frac{1}{2}$ apply to adding or subtracting an electron. Spin states of the molecule which differ by more than $\frac{1}{2}$ from the ground states are accessible via subsequent tunnel processes, but only if each step in the sequence is energetically allowed. A sequence of tunnel processes can result in a nonequilibrium population of certain excited states that can be depopulated only slowly by a violation of the spin-selection rules induced by QTM. Transport is then hindered or blocked at sufficiently low temperatures, leading to NDC or CCS.

Our calculations (see Fig. 4) take as a starting point the basic spin-Hamiltonian for a SMM in charge state N ($N = n$ neutral, $N = n - 1$ oxidized, $N = n + 1$ reduced) and two S states $\alpha = 0, 1$ for each charge state (energy splitting Δ_N) and total spin $S_{N\alpha}$:

$$H_{N\alpha} = -D_{N\alpha}S_z^2 + B_2(S_x^2 - S_y^2), \qquad (1)$$

where $D_{N\alpha} > 0$ is an anisotropy constant and B_2 the lowest order QTM perturbation due to deviations from perfect axial symmetry. For $B_2 = 0$, this Hamiltonian gives rise to a ladder consisting of the $2S_{N\alpha} + 1$ different M states; see Fig. 4(a). The states $M = \pm S_{N0}$ are degenerate ground states of the molecule and are separated by the magnetic anisotropy barrier (MAB). Transition rates between spin states upon adding or subtracting an electron are deter-
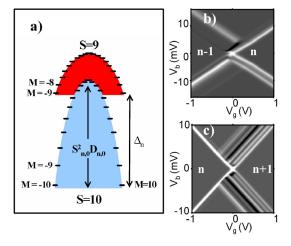
mined by Clebsch-Gordan coefficients and spin-selection rules. We consider weak QTM (small B_2) where this picture is still correct up to weak violations of the spin-selection rules which are taken into account. Electronic- and spin-excitation relaxation rates are assumed to be much smaller than the tunnel rates [26].

Measurements show that the MAB of the neutral Mn_{12} molecule ($D_{n0}S_{n0}^2$) equals 5.6 meV [8]. Recently, it has been demonstrated that the first excited spin state in a neutral Mn_{12} derivative has $S_{n,1} = 9$ and lies about $\Delta_n = 4$ meV above the $S_{n,0} = 10$ ground state [27], as theoretically predicted by Park and Pederson [28]. Little is known about positively or negatively charged Mn_{12} clusters, except that one-electron reduced species have a $S_{n+1,0} = 9\frac{1}{2}$ ground state and a lower MAB [29]. We therefore have performed calculations for various values of the remaining parameters and found that NDC and CCS are generic features whenever (i) the MAB is charge state dependent and (ii) the spin multiplets within a charge state overlap in energy ($D_{N0}S_{N0}^2 > \Delta_N$).

An example of CCS obtained from calculations is indicated in Fig. 4(b) for the $n - 1 \leftrightarrow n$ transition and parameters listed in Ref. [30]. In contrast to conventional spin blockade, the current is not blocked in the narrow region where only the ground states of the molecule are accessible. This is also observed experimentally. Excitations with NDC are obtained for the $n \leftrightarrow n + 1$ transition [see Fig. 4(c)]. The mechanism is similar as for CCS but requires a lower MAB of the charged ground state spin multiplet [30]. It is important to note that other parameter choices also give rise to CCS and NDC, so that a quantitative comparison cannot be made at the moment.

Other explanations for the NDC and CCS have also been considered. Both intrinsic and extrinsic (i.e., lead) properties could result in the observation of NDC. The observa-

tion of an NDC excitation in different samples implies that it results from an intrinsic property of the molecule, such as vibrational excitations. In some rather special situations, they are also predicted to result in NDC [31–34]. A CCS feature of the type observed here, however, has not been reported. Our model naturally gives rise to CCS and NDC due to the intrinsic properties of the magnetic molecule: charge induced distortion of the magnetic parameters and low-lying magnetic and spin excitations.

The low-energy features of the different transport regions in Fig. 2(a) are not identical, possibly because they correspond to different charge state transitions. In addition, the (magnetic) parameters may be affected by the different coupling to the electrodes. Since the lines in the transport regions correspond to sequences of transitions rather than to a single excitation, the pattern is sensitive to variations of the magnetic parameters (and other parameters such as temperature and tunnel coupling).

The effect of a magnetic field in transport experiments is much less obvious than in magnetic measurements on ensembles of molecules. First, the angle of the external field with respect to the easy axis of the molecule is unknown and cannot be controlled in our experimental setup. A transverse field leads to mixing of spin eigenstates, allowing transitions which are inhibited due to spin-selection rules in the absence of a field, whereas a longitudinal field will only shift the energies of the S_z states. However, estimates for the anisotropic g factors in the charge states are required to extend our basic model. Furthermore, the electron tunnel couplings can be modified by the field. The increase of the current upon applying a magnetic field [Fig. 2(b)] may be related to all of the above effects, but a full analysis of the magnetic field effects is beyond the scope of the present Letter.

In conclusion, we have measured transport through single Mn_{12} molecules that are weakly coupled to gold electrodes. Current suppression and negative differential conductance on the energy scale of the anisotropy barrier have been observed. These features can be understood qualitatively with a model that combines the spin properties of the molecule with standard sequential tunneling theory. These results provide a new direction in the study of single-molecule magnets and possibly lead to electronic control of nanomagnets.

---

*Electronic address: hubert@qt.tn.tudelft.nl

†Present Address: Department of Physics, University of British Columbia, Vancouver, Canada.

[1] J. Park *et al.*, Nature (London) **417,** 722 (2002).
[2] W. Liang *et al.*, Nature (London) **417,** 725 (2002).
[3] S. Kubatkin *et al.*, Nature (London) **425,** 698 (2003).
[4] H. Park *et al.*, Nature (London) **407,** 57 (2000).
[5] L. H. Yu *et al.*, Phys. Rev. Lett. **93,** 266802 (2004).
[6] A. N. Pasupathy *et al.*, Nano Lett. **5,** 203 (2005).
[7] R. Sessoli, D. Gatteschi, A. Caneschi, and M. A. Novak, Nature (London) **365,** 141 (1993).
[8] See EPAPS Document No. E-PRLTAO-96-043621 for more information on the synthesis and analysis of the Mn_{12} ($R = C_6H_4$) samples. For more information on EPAPS, see http://www.aip.org/pubservs/epaps.html.
[9] D. Gatteschi and R. Sessoli, Angew. Chem., Int. Ed. **42,** 268 (2003).
[10] J. R. Friedman, M. P. Sarachik, J. Tejada, and R. Ziolo, Phys. Rev. Lett. **76,** 3830 (1996).
[11] E. J. L. McInnes *et al.*, J. Am. Chem. Soc. **124,** 9219 (2002).
[12] M. Cavallini *et al.*, Angew. Chem., Int. Ed. **44,** 888 (2005).
[13] M. Mannini *et al.*, Nano Lett. **5,** 1435 (2005).
[14] K. Kim *et al.*, Appl. Phys. Lett. **85,** 3872 (2004).
[15] G.-H. Kim and T.-S. Kim, Phys. Rev. Lett. **92,** 137203 (2004).
[16] D. Weinmann, W. Häusler, and B. Kramer, Phys. Rev. Lett. **74,** 984 (1995).
[17] Hüttel *et al.*, Europhys. Lett. **62,** 712 (2003).
[18] A. Cornia *et al.*, Angew. Chem., Int. Ed. **42,** 1645 (2003).
[19] H. Park *et al.*, Appl. Phys. Lett. **75,** 301 (1999).
[20] The yield was similar for both types of derivatives. Two of the stable samples were obtained with the $R = C_{15}H_{30}$ derivative.
[21] M. R. Pederson, N. Bernstein, and J. Kortus, Phys. Rev. Lett. **89,** 097202 (2002).
[22] R. Sordan, K. Balasubramanian, M. Burghard, and K. Kern, Appl. Phys. Lett. **87,** 013106 (2005).
[23] A. A. Houck *et al.*, Nano Lett. **5,** 1685 (2005).
[24] H. B. Heersche *et al.*, Phys. Rev. Lett. **96,** 017205 (2006).
[25] H. van der Zant *et al.*, Faraday Discuss. **131,** 347 (2006).
[26] W. Wernsdorfer *et al.*, Europhys. Lett. **50,** 552 (2000).
[27] K. Petukhov *et al.*, Phys. Rev. B **70,** 054426 (2004).
[28] K. Park and M. R. Pederson, Phys. Rev. B **70,** 054414 (2004).
[29] N. Chakov *et al.*, Inorg. Chem. **44,** 5304 (2005).
[30] Model parameters (energies in [meV]) $(S_{n,0}, S_{n,1}) = (10, 9)$, $(D_{n,0}, D_{n,1}) = (0.056, 0.04)$, $\Delta_n = 4.0$, and $B_2 = 10^{-4}$. Parameters for CCS: $(S_{n-1,0}, S_{n-1,1}) = (9\frac{1}{2}, 9\frac{1}{2})$, $(D_{n-1,0}, D_{n-1,1}) = (0.02, 0.05)$, $\Delta_{n-1} = 1.3$, $\Gamma_L/\Gamma_R = 2$, and $T = 2$ K. Parameters for NDC: $(S_{n+1,0}, S_{n+1,1}) = (9\frac{1}{2}, 9\frac{1}{2})$, $(D_{n+1,0}, D_{n+1,1}) = (0.02, 0.02)$, $\Delta_{n+1} = 0.6$, $B_2 = 10^{-5}$, $\Gamma_L/\Gamma_R = 10$, and $T = 1$ K. The NDC *strength* can be reproduced only for a temperature lower than the experimental one in Figs. 2 and 3.
[31] J. Koch and F. von Oppen, Phys. Rev. Lett. **94,** 206804 (2005).
[32] M. R. Wegewijs and K. C. Nowack, New J. Phys. **7,** 239 (2005).
[33] K. C. Nowack and M. R. Wegewijs, cond-mat/0506552.
[34] A. Zazunov, D. Feinberg, and T. Martin, Phys. Rev. B **73,** 115405 (2006).